J. Fluid Mech. (1976), *vol.* 78, *part* 2, *pp.* 247–260
Printed in Great Britain

Some effects of inclination on elastohydrodynamic squeeze film problems

By D. WHICKER, A. L. BROWNE AND S. M. ROHDE

Engineering Mechanics Department, Research Laboratories, General Motors Corporation, Warren, Michigan 48090

(Received 17 November 1975 and in revised form 30 July 1976)

An analysis is presented for the non-inertial descent of an inclined sinkage element (a rectangular prism) through a viscous fluid onto a rigid surface. The effects of sinkage-element deformability, slip velocity and time-dependent loading conditions are considered. Unlike previous analyses no assumptions are made *a priori* about the form of the pressure distribution during, or the effect of corners on, inclined sinkage. The results for rigid square plates are compared with those of previous analyses and with the limited amount of experimental data available. Results are also presented for a deformable sinkage element, which is used to model the action of an individual tyre tread element on a wet pavement. An inclination function based on available data on the tyre surface shape in the footprint region is used. The loading function for this case is based on measured values of tyre footprint pressure.

1. Introduction

The approach of either a deformable and a rigid body or two deformable solids through an intervening viscous fluid is an essential feature of many lubrication and tyre traction problems. The theoretical contributions of Christensen (1961, 1970), Herrebrugh (1970) and Lee & Cheng (1973) to modelling such elastohydrodynamic (EHD) squeeze film problems all dealt with the hard EHD range. In the hard EHD range, the elastic moduli of the materials are sufficiently high that lubricant pressures capable of deforming them significantly will also substantially alter the lubricant's viscosity. The experimental work of Dowson & Jones (1967–68) dealt with this type of problem.

There has been a limited amount of work published concerning the squeeze film problem in the soft EHD range, where large deformations occur at low pressures. Several recent experimental investigations have dealt with this problem (Gaman, Higginson & Norman 1974; Roberts 1974). A theoretical analysis of the EHD squeeze film problem was presented by Rohde, Whicker & Browne (1976) and used to model the non-inertial descent of a tyre tread element onto a wet pavement (Browne, Whicker & Rohde 1975). The analysis by Browne *et al.* (1975) incorporated tread-element deformation, wheel slip and time-dependent loading. Previous tyre traction studies have treated the elements

as rigid (Browne 1975*b*; Bathelt 1973; Kienle 1974). The most frequently reported tread-element sinkage model, that of parallel sinkage, assumes the top of the tread element to be parallel to the plane of the pavement surface (Bathelt 1973; Kienle 1974). In Moore (1964) the expressions for parallel sinkage were modified for inclined sinkage by the introduction of a polynomial in the dimensionless angle of inclination. That theory neglected the pressure asymmetry caused by inclination of the plate. Some experimental results for the inclined sinkage of a flat plate in SAE 40 oil were also reported. Sinnamon & Tielking (1974) conducted some experiments with a rotating plate in an attempt to simulate certain features of a tyre rolling on a wet pavement. Inertial forces are important for the water depth and velocities at which their experiments were performed.

In this study we investigate the effects of inclination on the non-inertial descent of a sinkage element onto a smooth rigid surface. The approach used is based on that of Rohde *et al.* (1976) and Browne *et al.* (1975). Initially, we consider a rigid plate under constant load with an angle of inclination which varies linearly from a maximum value at the initial film thickness to a minimum value at zero (minimum) film thickness. We compare our results for this case with those presented by Moore (1964). Next we consider the case where the fluid pressure loading is constrained such that the equation of motion of an inertial mass in a direction normal to the rigid surface is satisfied. The results for this case are compared with the experimental data reported by Moore (1964). Finally, the analysis is used to simulate the descent of a tread element onto a pavement. The time dependence of the angle of inclination is based on the limited amount of tyre deformation data (Browne 1975*a*) available. A loading function based on tyre footprint pressure measurements (Browne *et al.* 1975; Lippmann & Oblizajek 1974) is considered.

2. Formulation

Consider the non-inertial descent of an inclined sinkage element onto a smooth rigid surface through a thin film of lubricant. The deformable sinkage element (figure 1) consists of an elastic layer of material bonded to a rigid surface. As the sinkage element descends (figure 2) it also rotates such that the angle of inclination at time t is $\Theta(t)$. We shall denote the initial and final values of $\Theta(t)$ by α and β, respectively. For the cases considered here, the angle of inclination $\Theta(t)$ is sufficiently small that we can make the small angle approximation ($\cos\Theta(t) = 1$) and set the co-ordinate X' along the inclined sinkage element equal to the co-ordinate X along the rigid surface. We consider only those cases for which the reduced Reynolds number R_e satisfies

$$R_e \equiv \frac{\rho h_m(0)\dot{h}}{\mu}\left(\frac{h_m(0)}{L}\right) < 1, \tag{1}$$

where $h_m(t) = H_m(t) - D$ (see also figures 1 and 2). Fluid inertial effects can then be neglected, and the intervening fluid is adequately characterized by the Reynolds equation

$$\nabla.\left(\frac{h^3}{12\mu}\nabla P\right) = \dot{h} + \frac{U}{2}\frac{\partial h}{\partial X}, \tag{2}$$

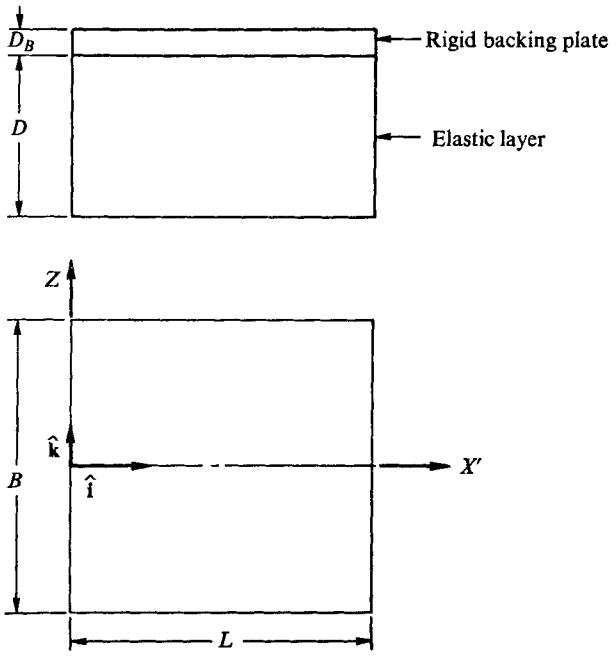

FIGURE 1. Sinkage-element geometry.

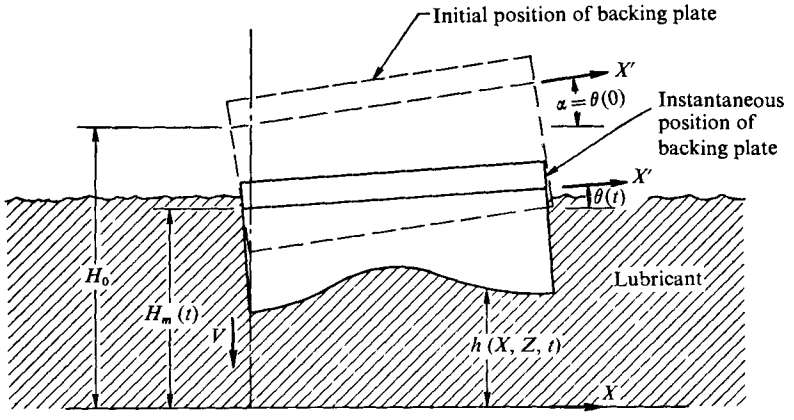

FIGURE 2. Motion of sinkage element.

where U is the slip velocity between the two surfaces. For the problems considered here, the fluid pressure levels are low enough that the fluid viscosity μ and density ρ may be treated as constants.

The thickness of the fluid film can be expressed as the sum of two factors:

$$h(X, Z, t) = h_0(X, t) + h_1(X, Z, t). \tag{3}$$

Here $h_0(X, t)$ is obtained by subtracting the undeformed thickness D of the elastic layer from the expression $h_B(X, t)$ for the height of the rigid backing surface:

$$h_0(X, t) = h_B(X, t) - D. \tag{4}$$

The remaining factor $h_1(X, Z, t)$ is the vertical displacement of the elastic layer owing to the pressure of the fluid film.

Following the approach of Rohde *et al.* (1976) and Browne *et al.* (1975), we introduce a linear operator $\mathscr{L}$ which relates the surface loading to the deformation of the elastic layer:†

$$h_1 = \mathscr{L}P. \tag{5a}$$

The expression for the film thickness now becomes

$$h(X, Z, t) = h_B(X, t) - D + \mathscr{L}P. \tag{5b}$$

Substituting this expression into Reynolds' equation, we obtain a single equation in P and h_0 which describes our elastohydrodynamic system:

$$\nabla . \left(\frac{(h_0 + \mathscr{L}P)^3}{12\mu} \nabla P \right) - \dot{h}_0 - \mathscr{L}\dot{P} - \frac{U}{2} \frac{\partial}{\partial X} (h_0 + \mathscr{L}P) = 0. \tag{6}$$

We seek a numerical solution of this equation. $\dot{P}$ and h_0 are approximated by the expressions

$$\dot{P}(X, Z, t) = [P(X, Z, t) - P(X, Z, t - \Delta t)]/\Delta t \tag{7a}$$

and

$$h_0(X, t + \Delta t) = h_0(X, t) + \Delta t \dot{h}_0(X, t). \tag{7b}$$

For the type of motion being considered here we have (figure 2)

$$h_0(X, t) = h_m(t) + X \tan \theta(t), \tag{8}$$

where $h_m(t) = H_m(t) - D$ (figure 2). For a known function $\Theta(t)$, the approximations (7) together with (8) reduce the number of dependent variables at time t to two: P and $h_m(t)$.

The boundary conditions for the rectangular region of solution $0 \leqslant X \leqslant L$, $0 \leqslant Z \leqslant \frac{1}{2}B$ are

$$\left.\begin{aligned} P &= 0 \quad \text{at} \quad X = 0, L \quad \text{for all } Z, \\ P &= 0 \quad \text{at} \quad Z = \tfrac{1}{2}B \quad \text{for all } X, \\ \partial P/\partial Z &= 0 \quad \text{at} \quad Z = 0 \quad \text{for all } X, \end{aligned}\right\} \tag{9}$$

where we have taken advantage of the symmetry about the X axis. The initial condition is

$$h_0(X, t) = h_m(0) + X \tan \alpha. \tag{10}$$

The system (5)–(10) can be solved subject to time-varying constraints on P and $\dot{h}_0$. Note that $\dot{h}_0$ can, in this sense, be regarded as a control which takes values such that functionals of the pressure satisfy the imposed constraints. Specific constraints considered in this study are constant load W,

$$\int_{-\frac{1}{2}B}^{\frac{1}{2}B} \int_0^L P(X, Z, t)\, dX\, dZ = W, \tag{11a}$$

time-varying-load $W(t)$,

$$\int_{-\frac{1}{2}B}^{\frac{1}{2}B} \int_0^L P(X, Z, t)\, dX\, dZ = W(t), \tag{11b}$$

† The X, Z and t dependences are to be understood.

and the vertical equation of motion for the element,

$$\int_{-\frac{1}{2}B}^{\frac{1}{2}B}\int_{0}^{L} P(X,Z,t)\,dX\,dZ = W + M_{\text{eff}}\frac{\partial^2 h_0}{\partial t^2}. \tag{11c}$$

Here M_{eff} is the effective mass of the sinkage element. For these constraints we replace (7*a*) at $t = 0$ with the condition $P(X,Z,0) = 0$. Otherwise, for

$$P(X,Z,0) > 0,$$

(7*a*) becomes indeterminate as $\Delta t \to 0$.

Equations (6)–(8), a specified function $\Theta(t)$ and one of the constraints (11) form a nonlinear integro-differential system of equations in $P(X,Z,t)$ and $\dot{h}_m(t)$ subject to the boundary and initial conditions (9) and (10). Substituting (7) and (8) into (6) and (11) we can rewrite (6) and (11) as the operator equations†

$$\alpha(P,\dot{h}_m) = 0, \quad \beta(P,\dot{h}_m) = 0, \tag{12}$$

subject to conditions (9) and (10).

Newton's method (Collatz 1966) is then used to construct solutions to (12). We let $\delta_n P$ and $\delta_n \dot{h}_m$ be solutions of the system of linear integro-differential equations

$$\left.\begin{aligned} \alpha(P^n,\dot{h}_m^n) + \partial_P \alpha(P^n,\dot{h}_m^n)\,\delta_n P + \partial_{\dot{h}_m}\alpha(P^n,\dot{h}_m^n)\,\delta_n \dot{h}_m = 0,\\ \beta(P^n,\dot{h}_m^n) + \partial_P \beta(P^n,\dot{h}_m^n)\,\delta_n P + \partial_{\dot{h}_m}\beta(P^n,\dot{h}_m^n)\,\delta_n \dot{h}_m = 0 \end{aligned}\right\} \tag{13}$$

and define $$P^{n+1} = P^n + \delta_n P, \quad \dot{h}_m^{n+1} = \dot{h}_m^n + \delta_n \dot{h}_m.$$

Here $\partial_P[\ ]$ and $\partial_{\dot{h}_m}[\ ]$ denote the Frechet derivatives of an operator with respect to P and $\dot{h}_m$ respectively. These derivatives (if they exist) at P and $\dot{h}_m$ are given by

$$\partial_P \mathcal{O}(P,\dot{h}_m)\,\delta P = \lim_{\epsilon\to 0}\left[\frac{d}{d\epsilon}\mathcal{O}(P+\epsilon\delta P,\dot{h}_m)\right],$$

$$\partial_{\dot{h}_m} \mathcal{O}(P,\dot{h}_m)\,\delta \dot{h}_m = \lim_{\epsilon\to 0}\left[\frac{d}{d\epsilon}\mathcal{O}(P,\dot{h}_m+\epsilon\delta \dot{h}_m)\right],$$

where $\mathcal{O}$ represents either the operator α or the operator β. For a given P_0 and $\dot{h}_m^0$, P_1 and $\dot{h}_m^1$ may be found by solving (13). If P_0 and $\dot{h}_m^0$ are in the region of attraction of the iterative scheme then the scheme will converge. For a detailed discussion of this method of solving operator equations see Collatz (1966).

The next step in the numerical solution of this system is to obtain an explicit discretized representation of the operator. The sinkage-element surface is subdivided into small rectangles of area LB/n^2. A three-dimensional finite-element analysis using hexahedral elements and linear interpolation functions is then used to determine the stiffness matrix $\mathbf{K}$ which relates the elastic displacements at the surface nodes to the fluid force acting on the sinkage-element surface. Then the nodal displacements $\mathbf{U}_1$ are related to the fluid force $\mathbf{F}$ by the expression

$$\mathbf{U}_1 = \mathbf{K}^{-1}\mathbf{F}, \tag{14a}$$

where $\mathbf{K}^{-1}$ is the compliance matrix.

† The dependence of P on X, Z and t and of h_m on t in (12) and in the subsequent discussion of the solution procedure is to be understood.

For a segment of the subdivided sinkage element, F is just

$$F = P(LB/n^2). \tag{14b}$$

Substituting (14*b*) into (14*a*) and non-dimensionalizing the resulting expression we obtain

$$\overline{U} \equiv U/h_m(0) = S\overline{K}^{-1}\overline{P},$$

where

$$S = \frac{500}{n^2}\frac{LB}{h_m(0)}\frac{P_{\text{ref}}}{E}, \quad \overline{K}^{-1} = \frac{E}{500}K^{-1},$$

P_{ref} is a reference pressure and E the Young's modulus of the elastic layer.

The linearized system (13) was discretized using the finite-difference method, and the operator $\mathscr{L}$ was replaced by its discrete representation $S\overline{K}^{-1}$. The resulting system of linear algebraic equations was then solved using Gaussian elimination.

The results for a deformable sinkage element presented here are for the geometry depicted in figure 1. This sinkage-element geometry is the same as that considered in Browne *et al.* (1975).

3. Rigid flat plate

This formulation was first employed to study the effect of inclination on the non-inertial descent of a rigid flat plate. The analysis for a rigid element is obtained by setting $S = 0$. We consider the same function for $\Theta(t)$ as did Moore (1964), that is

$$\Theta(t) = \frac{h_m(t)}{h_m(0)}(\alpha - \beta) + \beta. \tag{15}$$

The following set of parameter values was used for this case:

$$L = 229\,\text{mm}, \quad h_m(0) = 6{\cdot}35\,\text{mm}, \quad n = 8,$$
$$\mu = 0{\cdot}4137\,\text{N s/m}^2, \quad P_{\text{ref}} = 9{\cdot}38 \times 10^{-2}\,\text{kPa},$$
$$\mu/\rho = 4{\cdot}3 \times 10^{-5}\,\text{m}^2/\text{s}.$$

The interfacial lubricant to which these parameter values correspond is SAE 40 oil at 77 °F. Substituting this set of parameters in (1), we find that, for this case, where the sinkage velocity is of the order of 10^{-1} m/s, fluid inertial effects can be neglected.

We denote the centre-point film thickness by h_c and define the average sinkage velocity V_{sink} by

$$V_{\text{sink}} = -\frac{1}{L}\int_0^L \frac{\partial h(X,t)}{\partial t}\,dX. \tag{16}$$

Characteristic curves of average sinkage velocity *vs.* h_c^3 for parallel and inclined plates under a constant load of 4·89 N are shown in figure 3. The corresponding results obtained using the treatment of Moore (1964) are plotted here for comparison. For parallel surfaces ($\Theta(t) \equiv 0$), both solution procedures yield results in agreement with those obtained by Hays (1962).† For all other cases considered,

† Note that Moore (1964) arbitrarily introduced a constant in the expression for the sinkage rate, so that this expression agreed with that obtained by Hays (1962).

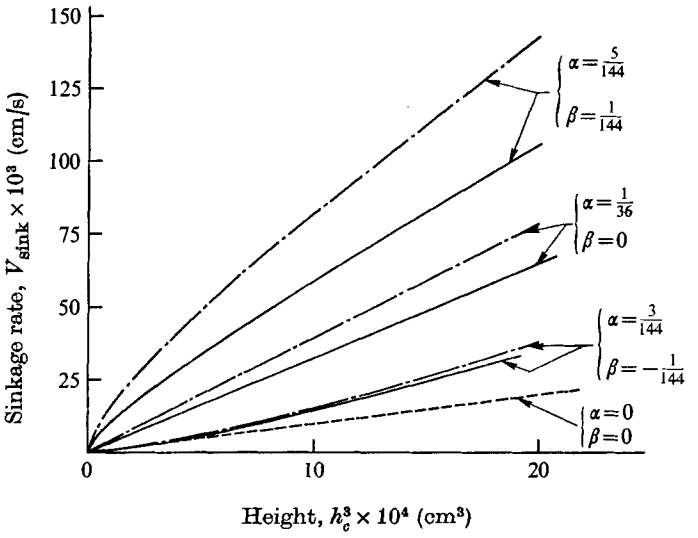

FIGURE 3. Comparison of predicted sinkage velocity with theory of Moore (1964). ——, Browne *et al.*; — · —, Moore. Load = 4·89 N.

the procedure of Moore (1964) predicts higher values for the sinkage velocity. Moore's (1964) treatment is based on the assumptions (i) that the corner effects for an inclined square plate are the same as the corner effects for a parallel square plate and (ii) that the asymmetry of the pressure distribution caused by plate inclination is negligible. On the basis of the rather dubious assumption that the distance the point of maximum pressure moves towards the leading edge is equal to the distance between the centre of gravity and centre of pressure, Moore (1964) concludes that the former distance is about $0{\cdot}015L$. He therefore neglects the effects of pressure asymmetry. We have found, however, that inclination results in a significant asymmetry of the pressure distribution. The centre-line pressure distribution across an inclined plate is plotted in figure 4. The point of maximum pressure has moved a distance of over $0{\cdot}15L$ towards the leading edge.

Characteristic V_{sink} *vs.* h_c^3 curves for several (constant) loads are presented in figure 5. The results predicted by the theory presented by Moore (1964) for these cases are also plotted along with some experimental data reported by Moore (1964). The experimental apparatus used by Moore (1964) consisted of a mechanical linkage carrying a heavy square plate at one end and a system of counterweights at the other end. The applied load for such an apparatus is actually equal to the weight excess of the plate (over the counterweights) plus an inertial term due to the acceleration of all of the masses. It should also be noted that with this counterweight system the mass to be accelerated increases as the load is decreased (by adding counterweights). Equation (11*c*) is the appropriate constraint for this case. We introduce the approximation

$$\ddot{h}_m(t) = [\dot{h}_m(t) - \dot{h}_m(t-\Delta t)]/\Delta t$$

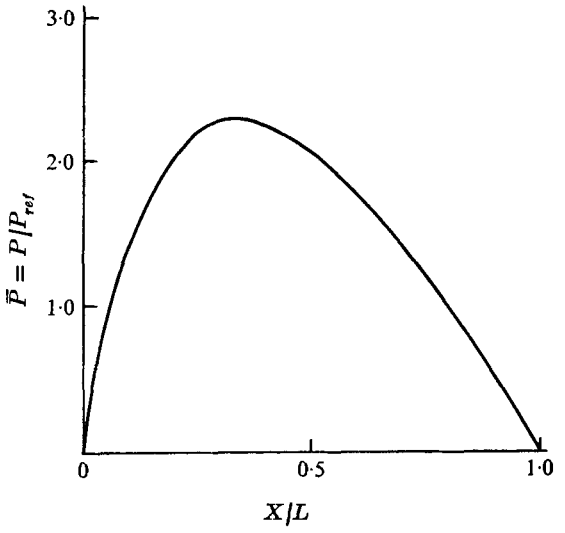

FIGURE 4. Centre-line pressure distribution. $\alpha = \frac{1}{36}$, $\beta = 0$, $L = 229$ mm, SAE 40 oil at 77 °F, $\bar{W} \equiv W/(P_{ref}L)^2 = 1{\cdot}0$, $h_m(0) = 6{\cdot}35$ mm.

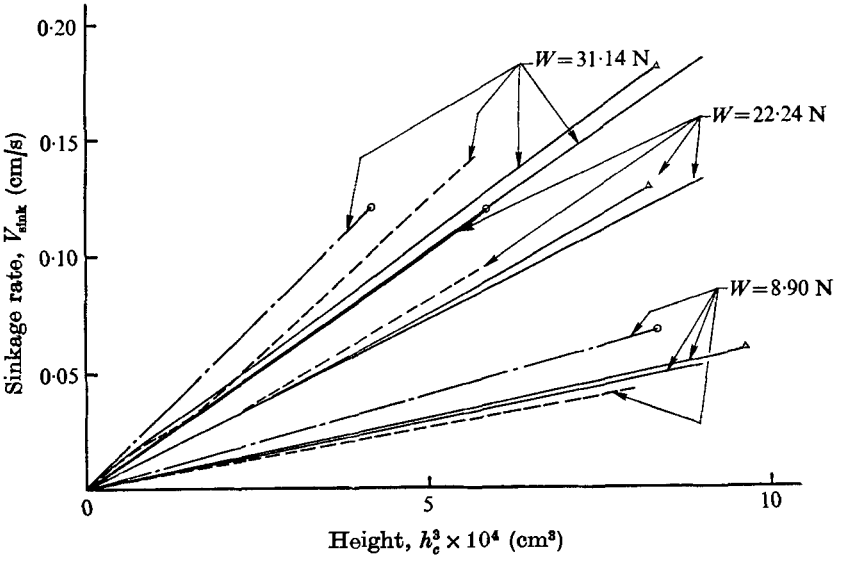

FIGURE 5. Sinkage velocity: comparison of theory with experiment. ——, theory (Browne *et al.*); △—△, inertial theory (Browne *et al.*); – – –, experiment (Moore); ○—·—○, theory (Moore). Values of all parameters except W as in figure 4.

and solve the system (6)–(10) subject to the constraint (11*c*). Since no detailed information about the linkage mass and moment of inertia was available, only the inertial effects of the plate and counterweights were considered. The results of an analysis incorporating these effects are plotted in figure 5. For all three weights, the inertially constrained theory predicts values which are in closer agreement with the reported experimental data than are values based on the

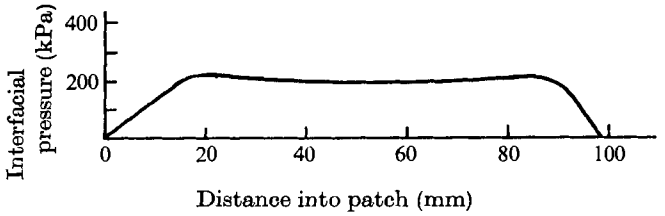

FIGURE 6. Interfacial pressure distribution BBPC2 under tread rib for dry contact and free rolling at zero camber and steer at an inflation pressure of 179 kPa; 100 % tyre and rim association load of 7030 N, size H tyre. From Lippmann & Oblizajek (1974). BBP, belted bias ply tyre; C, centre rib; 2, correction for effect of upstream water film.

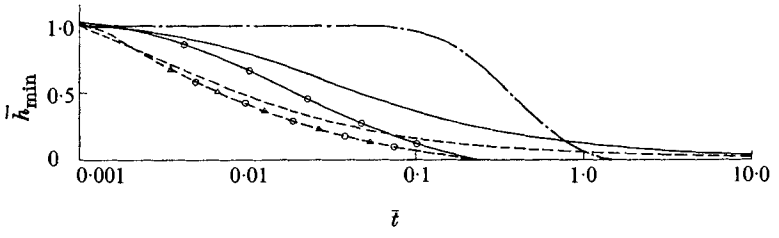

FIGURE 7. Time histories of the minimum film thickness. ——, rigid, parallel, constant load, no slip ($S = 0$, $\alpha = \beta = 0$, $\overline{W} = 1{\cdot}0$, $U = 0$); —○—, flexible, parallel, constant load, no slip ($S = 83{\cdot}705$, $\alpha = \beta = 0$, $\overline{W} = 1{\cdot}0$, $U = 0$); – – –, rigid, rotating, constant load, no slip ($S = 0$, $\alpha = \frac{1}{360}$, $\beta = 0$, $\overline{W} = 1{\cdot}0$, $U = 0$); – –○– –, flexible, rotating, constant load, no slip ($S = 83{\cdot}705$, $\alpha = \frac{1}{360}$, $\beta = 0$, $\overline{W} = 1{\cdot}0$, $U = 0$); – – △– –, flexible, rotating, constant load, slip ($S = 83{\cdot}705$, $\alpha = \frac{1}{360}$, $\beta = 0$, $\overline{W} = 1{\cdot}0$, $U = 0{\cdot}87$ m/s); — · —, flexible, rotating, varying load, no slip ($S = 83{\cdot}705$, $\Theta(\bar{t})$ from moiré data, BBPC2, $U = 0$).

theory of Moore (1964). For the 8·9 N load the best agreement is obtained by neglecting the inertial effects of the weights and plate. Any friction in the linkage or other experimental error would be most significant for this case.

4. Deformable sinkage element

The analysis was next applied to a deformable sinkage element identical to that used by Browne *et al.* (1975) to model the action of a tyre tread element. The parameters used for this case were

$$L = 19{\cdot}05\,\text{mm}, \quad D = 9{\cdot}525\,\text{mm}, \quad n = 8,$$
$$h_m(0) = 0{\cdot}18\,\text{mm}, \quad \mu = 9{\cdot}6 \times 10^{-4}\,\text{N s/m}^2,$$
$$\mu/\rho = 9{\cdot}3 \times 10^{-7}\,\text{m}^2/\text{s}, \quad P_{\text{ref}} = 344{\cdot}7\,\text{kPa}, \quad E = 2585\,\text{kPa}, \quad \nu = 0{\cdot}499.$$

For these parameters and the velocity range considered, (1) is clearly satisfied.

Two types of inclination history were considered. For the first one, $\Theta(t)$ is given by (15) for $h_m(t) > 0$. For $h_m(t) \leqslant 0$, $\Theta(t) = \beta$. The second inclination history was based on the moiré data of Browne (1975*a*). The two pressure constraints considered were those of constant load and the loading function depicted in figure 6. This loading function is based on the tyre footprint pressure data of Lippmann & Oblizajek (1974) modified as described in Browne *et al.* (1975) to account for the presence of the fluid film. The effect of a slip velocity of 0·87 m/s

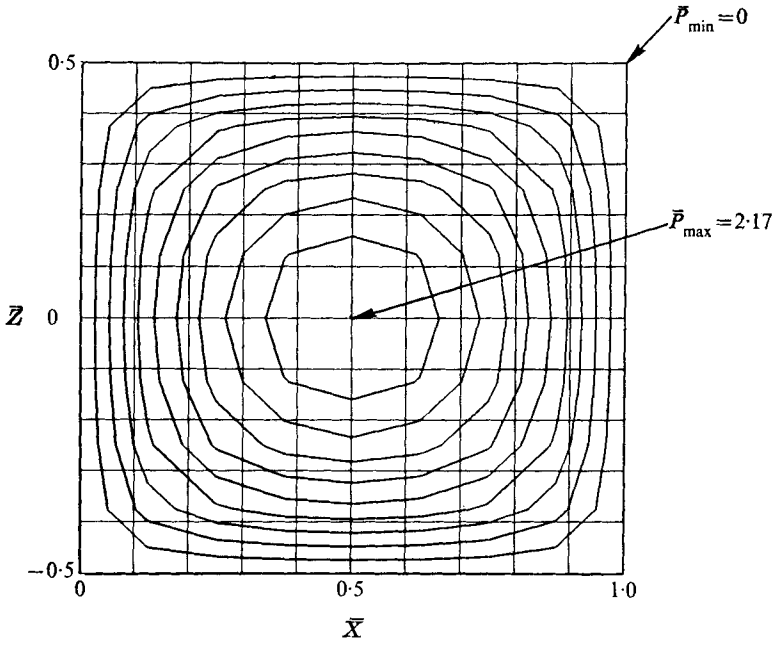

FIGURE 8. Representative pressure distribution for parallel sinkage of a rigid element; $\bar{W} = 1{\cdot}0$, contour interval = 0·217. $\bar{X} \equiv X/L$, $\bar{Z} = Z/L$.

was also considered. Time histories of the minimum film thickness are plotted in figure 7. Time histories of the minimum film thickness for rigid parallel and deformable parallel sinkage are included for comparison purposes. For this representative set of tread-element parameters, the slip velocity of 0·87 m/s has no significant effect on the sinkage behaviour of the element.

The effect of inclination is most pronounced during the initial stage of sinkage, i.e. when $\Theta(t)$ is largest. The total sinkage time is more strongly influenced by whether the sinkage element is rigid or deformable than by the inclination histories considered. For the deformable element, the increase in velocity due to inclination results in the formation of a larger pocket. After this pocket has formed and trapped fluid, the sinkage velocity for inclined sinkage actually drops below that for parallel sinkage.

Figure 8 shows a contour plot of the pressure distribution for the parallel sinkage of a rigid element under constant load. Figure 9(*a*) shows a contour plot of pressure for parallel sinkage of a deformable element under the same constant load. A contour plot of the corresponding film thickness is given in figure 9(*b*). Comparison of figure 9 (*a*) with figure 8 shows clearly how the pocket traps fluid and increases the area of the high pressure fluid region.

A contour plot of the pressure distribution for inclined sinkage [$\Theta(t)$ given by (15)] of a rigid element under constant load is given in figure 10. Comparison of figure 10 with figure 8 clearly shows how inclination causes asymmetry of the pressure distribution. Figure 11 (*a*) is a contour plot of the pressure for a deformable element under the same constraint. A contour plot of the corresponding

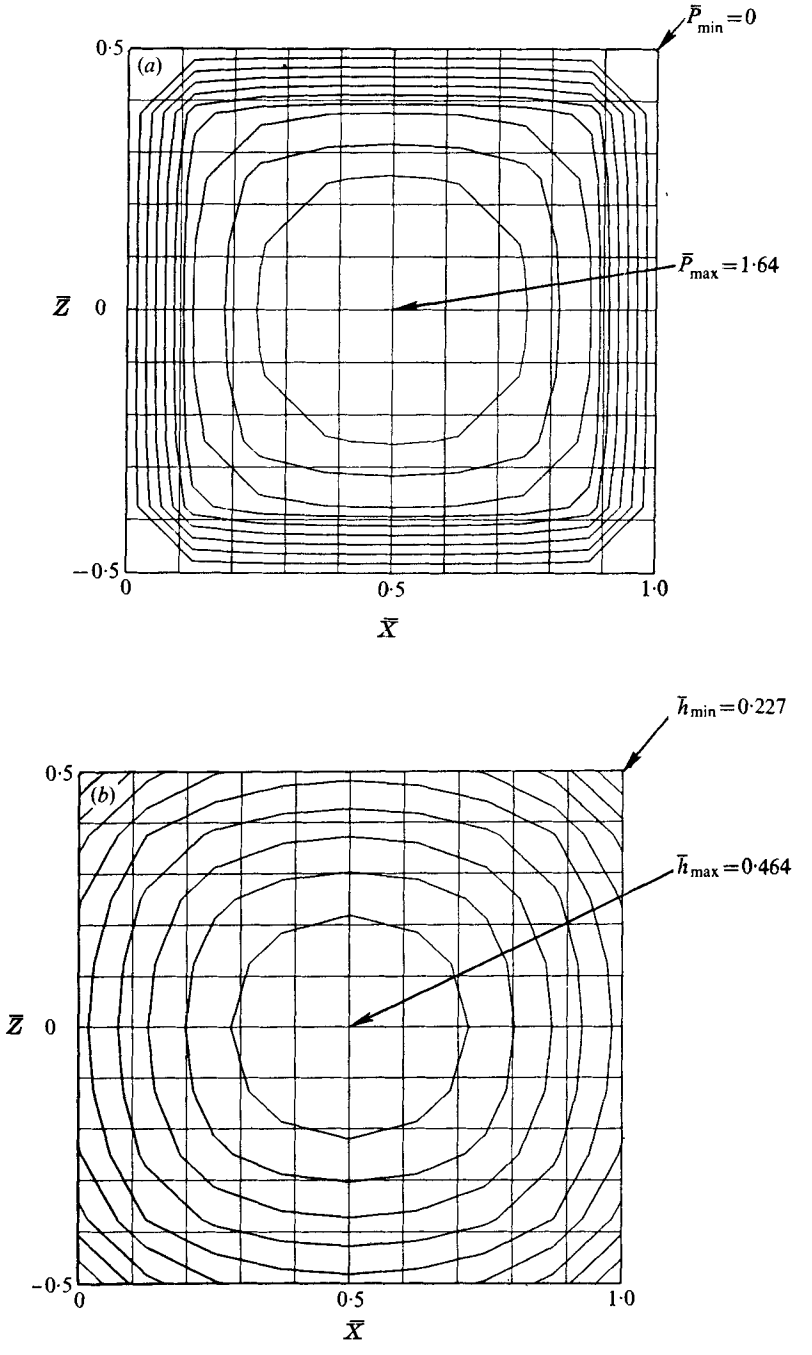

FIGURE 9. (*a*) Representative pressure distribution and (*b*) film-thickness distribution for parallel sinkage of a deformable element; $\overline{W} = 1·0$, $S = 83·75$. (*a*) Contour interval = 0·164. (*b*) Contour interval = 0·0237.

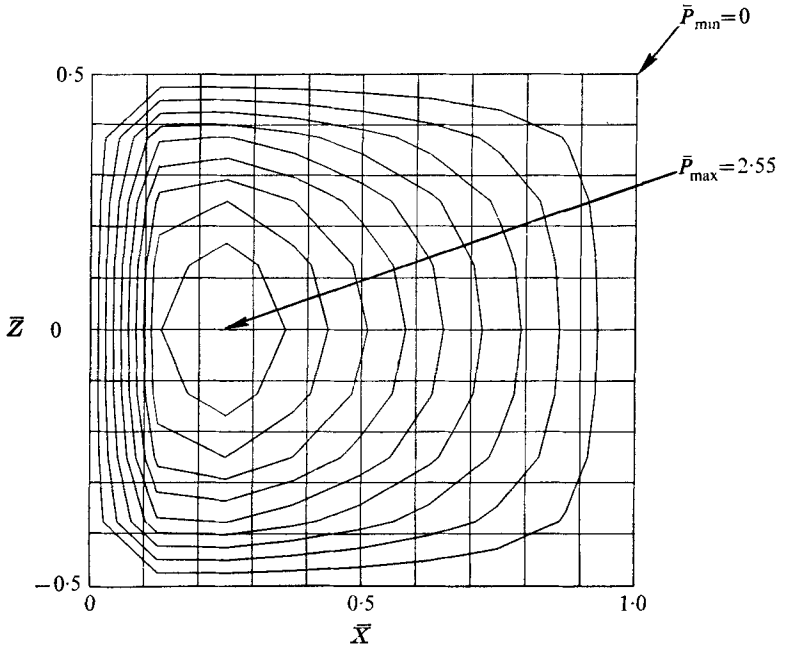

FIGURE 10. Representative pressure distribution for inclined sinkage of a rigid element; $\overline{W} = 1{\cdot}0$, $\alpha = 0{\cdot}02778$, $\beta = 0$, contour interval = 0·255.

film thickness is shown in figure 11(*b*). The influence of the deformation pocket on the pressure distribution of figure 11 (*a*) is clearly visible.

5. Discussion

An analysis has been presented for the inclined non-inertial descent of a sinkage element onto a rigid surface. The effects of deformation of the element, slip velocity and time-dependent loading conditions were considered. Contrary to the assumption of Moore (1964), inclination results in significant asymmetry of the pressure distribution. The centre of pressure may move by as much as 15 % of the length of the inclined sinkage element. The assumption by Moore that corner effects for an inclined square plate are the same as for a parallel square plate is, at best, reasonable for only a very restricted range of inclination angles.

Inclination was found to result in a dramatic increase in the initial sinkage velocity. For a rigid element, the sinkage velocity approaches that for parallel sinkage as the angle of inclination $\Theta(t)$ decreases. For a deformable element the initial velocity increase results in a larger deformation pocket. This pocket traps more fluid and quickly reduces the sinkage velocity. For the range of parameters considered, the sinkage velocity was reduced below that for parallel sinkage. In summary, the total sinkage time was more strongly influenced by whether the sinkage element was deformable or rigid than by whether or not there was inclination.

The results for a deformable sinkage element presented here and in Browne *et al.* (1975) are of particular interest in the area of tyre traction. A deformable

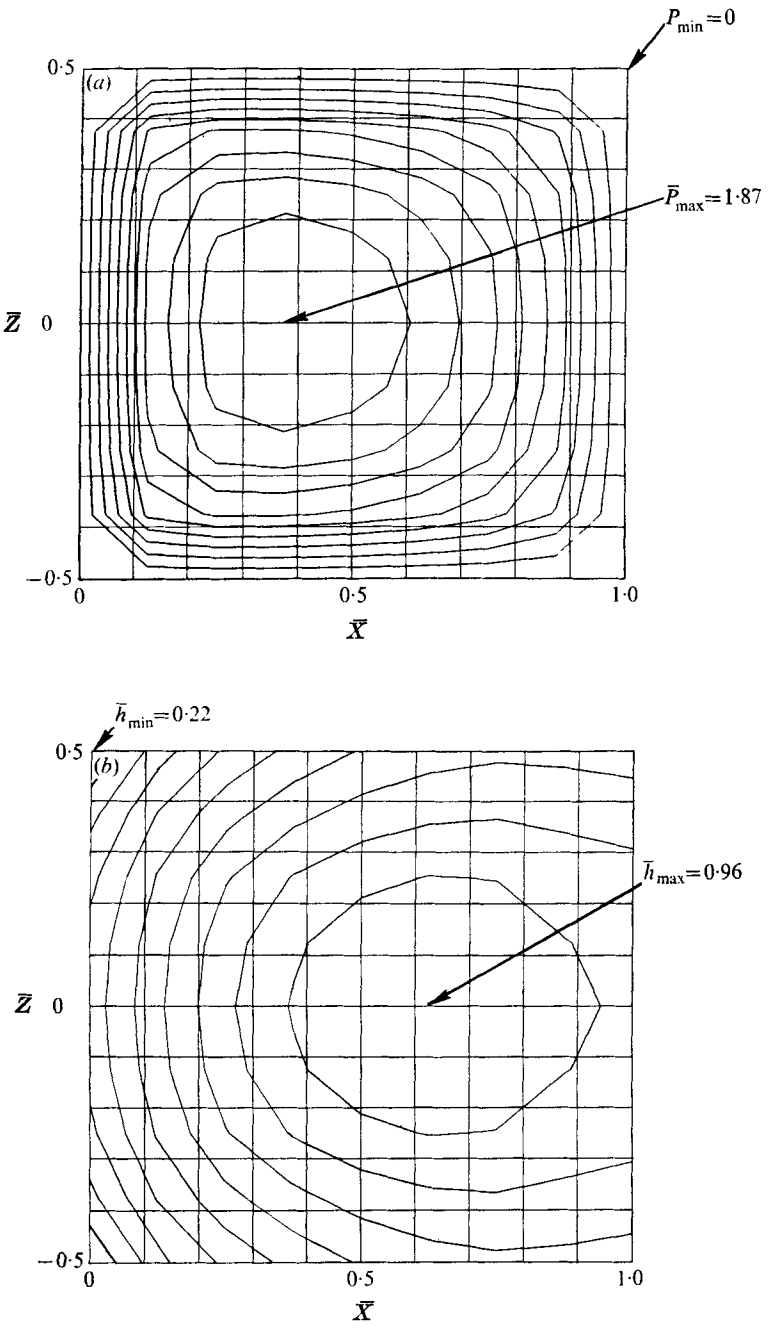

FIGURE 11. (*a*) Representative pressure distribution and (*b*) film-thickness distribution for inclined sinkage of a deformable element; $\overline{W} = 1·0$, $\alpha = 0·02778$, $\beta = 0$, $S = 83·705$. (*a*) Contour interval = 0·187. (*b*) Contour interval = 0·096.

tread element is found to descend rapidly through the fluid film until initial contact occurs at the tread element's corners. Available tyre traction is strongly dependent on whether or not there is sufficient pavement microtexture (Rohde 1976) to allow the fluid trapped between the tread element and the pavement surface to escape. Varying such parameters as slip velocity and surface inclination results in changes in the time to initial contact which are small compared with the changes found in going from a rigid-plate model to a deformable-element model. Both the slip velocity and the surface inclination, however, result in changes in the pressure distribution and consequently in the shape and depth of the deformation pocket. The effect of such changes, if any, on traction production requires a more detailed understanding of the post-contact phase of tread-element performance. An investigation of this post-contact phase is currently underway.

REFERENCES

BATHELT, H. 1973 Calculation of the aquaplaning behaviour of smooth and profiled tires. *ATZ Int.* **75** (10), 12–17.

BROWNE, A. L. 1975*a* Tire deformation during dynamic hydroplaning. *Tire Sci. Tech.* **3**, 16–28.

BROWNE, A. L. 1975*b* Mathematical analysis for pneumatic tire hydroplaning. *A.S.T.M.* STP-583, 75–94.

BROWNE, A. L., WHICKER, D. & ROHDE, S. M. 1975 The significance of tread element flexibility to thin film wet traction. *Tire Sci. Tech.* **3**, 215–234.

CHRISTENSEN, H. 1961 The oil film in a closing gap. *Proc. Roy. Soc.* A **266**, 312–328.

CHRISTENSEN, H. 1970 Elastohydrodynamic theory of spherical bodies in normal approach. *Trans. A.S.M.E.* F **92**, 145–154.

COLLATZ, L. 1966 *Functional Analysis and Numerical Mathematics.* Academic.

DOWSON, D. & JONES, D. A. 1967–68 An optical-interference method of measurement of time-dependent elastohydrodynamic oil film profiles. *Proc. Inst. Mech. Engrs*, **182**, 3G.

GAMAN, I. D. C., HIGGINSON, G. R. & NORMAN, R. 1974 Fluid entrapment by a soft surface layer. *Wear*, **28**, 345–352.

HAYS, D. F. 1962 Squeeze films for rectangular plates. *A.S.M.E. Paper*, no. 62-LubS-9.

HERREBRUGH, K. 1970 Elastohydrodynamic squeeze films between two cylinders in normal approach. *Trans. A.S.M.E.* F **92**, 292–302.

KIENLE, R. N. 1974 In *The Physics of Tire Traction: Theory and Experiment* (ed. D. F. Hays & A. L. Browne), pp. 241–255. Plenum.

LEE, K. M. & CHENG, H. S. 1973 The pressure and deformation profiles between two normally approaching lubricated cylinders. *Trans. A.S.M.E.* F **95**, 308–320.

LIPPMANN, S. A. & OBLIZAJEK, K. L. 1974 The distributions of stress between the tread and the road for freely rolling tires. *S.A.E. Paper*, no. 740072.

MOORE, D. F. 1964 On the inclined non-inertial sinkage of a flat plate. *J. Fluid Mech.* **20**, 321–330.

ROBERTS, A. D. 1974 In *The Physics of Tire Traction: Theory and Experiment* (ed. D. F. Hays & A. L. Browne), pp. 179–194. Plenum.

ROHDE, S. M. 1976 On the effect of pavement microtexture on thin film wet traction. *Int. J. Mech. Sci.* **18**, 95–101.

ROHDE, S. M., WHICKER, D. & BROWNE, A. L. 1976 Dynamic analysis of elastohydrodynamic squeeze films. *Trans. A.S.M.E.* F **98**, 401–408.

SINNAMON, J. F. & TIELKING, J. T. 1974 Hydroplaning and tread pattern hydrodynamics. *Univ. Michigan, Highway Safety Res. Inst. Rep.* no. UM-HSRI-PF-74-10.